Conference Paper

Direct Measurement of Built-in Electrical Potential in Photovoltaic Devices by Scanning Kelvin Probe Microscopy

C.S. Jiang, H.R. Moutinho, F.S. Hasoon,
H.A. Al-Thani, D.J. Friedman, J.F. Geisz,
Q. Wang, M.J. Romero, and M.M. Al-Jassim

NREL

National Renewable Energy Laboratory

Available electronically at http://www.osti.gov/bridge

Available for a processing fee to U.S. Department of Energy
and its contractors, in paper, from:
      U.S. Department of Energy
      Office of Scientific and Technical Information
      P.O. Box 62
      Oak Ridge, TN 37831-0062
      phone: 865.576.8401
      fax: 865.576.5728
      email: reports@adonis.osti.gov

Available for sale to the public, in paper, from:
      U.S. Department of Commerce
      National Technical Information Service
      5285 Port Royal Road
      Springfield, VA 22161
      phone: 800.553.6847
      fax: 703.605.6900
      email: orders@ntis.fedworld.gov
      online ordering: http://www.ntis.gov/ordering.htm

Printed on paper containing at least 50% wastepaper, including 20% postconsumer waste

Direct Measurement of Built-in Electrical Potential in Photovoltaic Devices by Scanning Kelvin Probe Microscopy

C.-S. Jiang, H. R. Moutinho, F.S. Hasoon, H.A. Al-Thani, D. J. Friedman, J. F. Geisz, Q. Wang, M.J. Romero, and M. M. Al-Jassim

National Renewable Energy Laboratory, 1617 Cole Blvd, Golden, CO 80401

ABSTRACT

We report on direct measurements of the built-in electrical potential in Cu(In,Ga)Se$_2$, GaInP$_2$ single-junction, and GaInP$_2$/GaAs tandem-junction solar cells, by using scanning Kelvin probe microscopy. Potential profiles on cross sections of the devices were measured quantitatively and spatially resolved in open and short circuit, under and without illuminations, with selective photon energies matching the band gaps of the junctions. The measurements provide valuable information about the electrical properties of the devices and are useful for understanding the performance and improving the design of solar cells.

1. Introduction

The built-in electric potential plays a major role in photovoltaic devices, because it collects photo-excited carriers and is a key factor in determining the open-circuit voltage (V_{oc}) of the device. However, characterization of the built-in potentials has been limited to indirect ways, such as current-voltage (I-V) and capacitance-voltage (C-V) measurements. Based on the complexity of modern solar cell devices with multiple interfaces, indirect measurement is inadequate to allocate the p-n junction positions and cannot distinguish contributions from the multiple layers of the devices. A direct measurement of the built-in potential with spatially resolved capabilities is highly desirable for understanding the performance and improving design of solar cells.

In the last decade, nano-electrical property measurements based on the atomic force microscopy (AFM) technique, such as scanning Kelvin probe microscopy (SKPM) and scanning capacitance microscopy (SCM), have been developed and applied to the characterization of semiconductor devices. Recently, we have applied SKPM and SCM to the characterization of photovoltaic devices. We measured the potential distributions on cross sections of thin-film solar cells of Cu(In,Ca)Se$_2$ (CIGS), amorphous-Si, and epitaxial III-V cells of GaInP$_2$, GaNPAs, and GaInP$_2$/GaAs [1-3]. In this paper, we will report briefly on the measurement technique and on potential measurements for three examples of CIGS, GaInP$_2$ single-junction, and GaInP$_2$/GaAs tandem-junction cells.

2. Measurement Technique

We used the SKPM technique (Fig. 1) and quantitatively measured the distribution of the electrochemical potential on cross sections of solar cell devices. In addition to the atomic force between the AFM tip and the sample surface, which gives a two-dimensional topographic image of the surface, there is a Coulomb interaction between the tip and the sample. To enhance the Coulomb interaction, an ac voltage is applied to the tip. The Coulomb force can be described as:

$$F = F_0 + F_1 + F_2$$

$$F_0 = \frac{1}{2}\frac{\partial C}{\partial z}\left[(V_{tip} - V_s)^2 + \frac{1}{2}V_{ac}^2\right]$$

$$F_1 = \frac{\partial C}{\partial z}(V_{tip} - V_s)V_{ac}\ \sin(\omega t)$$

$$F_2 = -\frac{1}{4}\frac{\partial C}{\partial z}V_{ac}^2\ \cos(2\omega t)$$

where C, V_{tip}, V_s, and V_{ac} are the capacitance between the tip and the sample, the electrochemical potentials of the tip and the sample surface, and the amplitude of the ac voltage, respectively. Using a lock-in-amplifier, the second term in the equation, F_1, is detected. The signal is sent to a negative feedback loop, and an instant dc voltage proportional to the force F_1 is summed to the tip. By the negative feedback V_{tip} is always adjusted to be equal to V_s, and the force F_1 is nullified. In this way, the electrochemical potential and the topography of the sample are imaged simultaneously.

For the III-V devices, atomically flat (110) cross-sectional surfaces were obtained by cleaving the (001) wafer along the $[1\bar{1}0]$ direction in air. To get flat cross sections of CIGS devices, which is necessary to avoid the convolution of topographic roughness to the SKPM signal, we grew the device structure on a Mo-coated GaAs(001) wafer instead of soda lime silicate glass. When we incorporated Na using a NaF source during the growth of the CIGS film, I-V characterization showed identical properties to the devices grown on the glass substrates. The potential was measured under conditions of open circuit (OC) or short circuit (SC). To measure the photo-response of the potential, a halogen lamp is irradiated at the front surface of the device. We used glass filters with either high- or low-wavelength passes to match the photon energy to the band gaps of the solar cells.
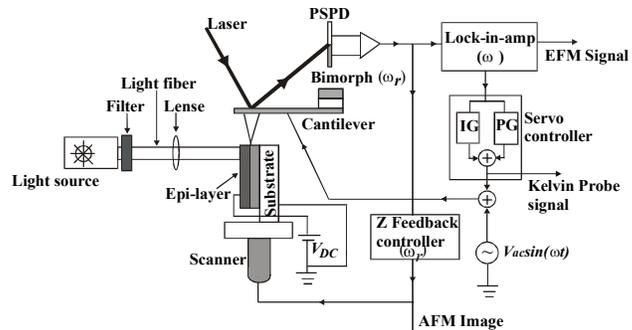

Figure 1. Schematic of the SKPM measurement system on cross sections of solar cell devices.

3. CIGS Solar Cells

Figure 2(a) shows an AFM image of the cross-sectional surface of the CIGS device. The CIGS film appears to consist of large grains, in contrast to the CdS/ZnO region.

This difference in grain size reveals a boundary between the CIGS and CdS/ZnO regions. However, the boundary between the CdS and ZnO layers is not discernible from the topographic image. The corresponding SKPM image taken in a reverse-bias voltage of Vb=1 V [Fig. 2(b)] shows a boundary of contrast that is consistent with the boundary shape of CIGS/CdS [Fig. 2(a)]. To reveal the SKPM and AFM features in detail, example line profiles along the same line scan, as indicated in both images, are shown in Fig. 2(c). From the AFM profile, we determined the location of the CIGS/CdS interface, as indicated by the dotted circles in the figures. Because the external voltage is a reverse bias, the potential in the CdS and ZnO regions is higher than in the CIGS region. The potential starts to drop at the interface and extends to ~250 nm into the CIGS film. This demonstrates that a built-in electric field exists on the CIGS side close to the interface, and the p-n junction is located at a location of 0–250 nm from the interface.

To determine the p/n boundary of the junction, we take the first differential of the potential profile [Fig. 2(c)]. This corresponds to the strength of the electric field, and the location of maximum electric field corresponds to the p/n boundary. In the present line scan, it is located ~60 nm from the CIGS/CdS interface. In all the effective line scans that have good SKPM signal/noise levels, and in which the location of the GIGS/CdS interface can be determined from the AFM profile, the p/n boundary is located 30–80 nm from the CIGS/CdS interface. Also shown in Fig. 1(c) is a SKPM line profile taken in OC at the same line position. The potential profile is relatively flat over the CIGS, CdS, and ZnO layers. The reason that we did not probe the potential variation on the p-n junction in the condition of OC is due possibly to surface Fermi level (E_F) pinning. We cleaved the sample and measured the SKPM in air; absorption of air molecules on the sample surface may cause the pinning of E_F and neutralize the difference in the work function between the p and n regions. Such effects of surface E_F pinning are widely reported and also showed up in our SKPM measurements on other samples.

With an external voltage applied to the p-n junction, SKPM can measure the potential drop because the voltage does not unpin the surface E_F. The "intrinsic" potential height in the bulk without an external voltage is slightly smaller than the energy band gap (1.12 eV). To make the potential height on the surface similar to that of the bulk in the "intrinsic" case without an external voltage, we applied the reverse-bias voltage of 1 V, and found that it reveals the p-n junction properly. Depletion widths of 60 nm in the n-region and 190 nm in the p-region correspond to a doping level of ~2×10^{17} and ~6×10^{16}/cm^3, respectively, by taking a dielectric constant of ε=12 and band gap of 1.12 eV. The bulk of the CIGS film fabricated by "three-stage co-evaporation" is p-type. The n-type region close to the CIGS/CdS interface may be doped by the diffusion of Cd^{2+} during the formation of the CdS layer and post-anneals [4]. These Cd^{2+} ions would occupy Cu sites and act as donors.

4. GaInP$_2$ Single-Junction Cells

Figure 3 shows an AFM image and the corresponding SKPM image taken on cross sections of GaInP$_2$ cells in OC. A potential profile, which is an average of the SKPM image over the lateral direction (parallel to the front surface of the device), is shown in Fig. 3(c). Another potential profile taken under SC is also shown in the figure. On both potential profiles in OC and SC, there are three main features: (1) the potentials show identical broad decreases (~350 mV) near the GaInP$_2$/GaAs interface; (2) they increase at the p-n junction; and (3) the increase of potential at the p-n junction saturates near the sample front surface and shows a small terrace or saddle shape. The increase at the p-n junction is different between OC and SC. It increases slowly in OC and steeply in SC.

The saturation of the potential increase seems to be caused by the effects of sample edge [1]. We extrapolate the potential profiles to calibrate the increasing amount in the region of the p-n junction, as shown in Fig. 3(c) by dotted lines. Both OC and SC are in thermal equilibrium state and should give identical potential profiles if there is no illumination on the sample. However, they show a big difference in the potential difference at the p-n junction, ~250 mV for OC and ~780 mV for SC. This is because AFM uses a laser to probe the deflections of the cantilever, and illumination of the laser light on the samples cannot be avoided at this stage. This unintended illumination produces a V_{oc} of 630 mV.
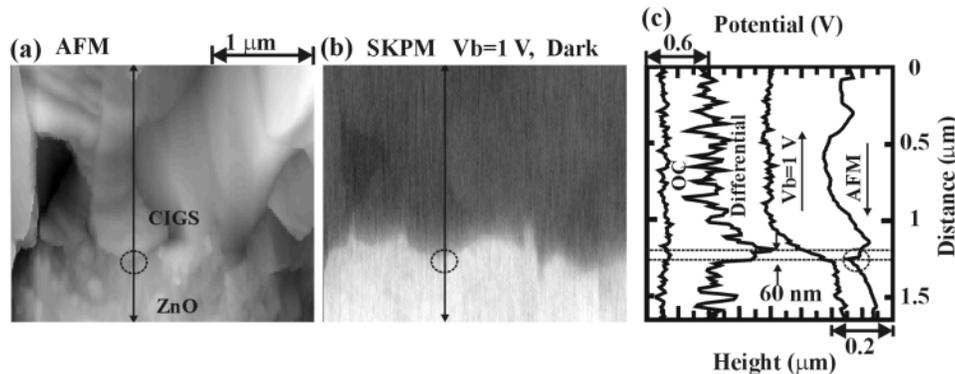

Figure 2. AFM (a) and corresponding SKPM (b) images of a CIGS solar cell taken in a reverse-bias voltage of 1 V. Example line scan profiles along the line indicated in (a) and (b) are shown in (c). A potential profile taken in OC is also shown in (c).
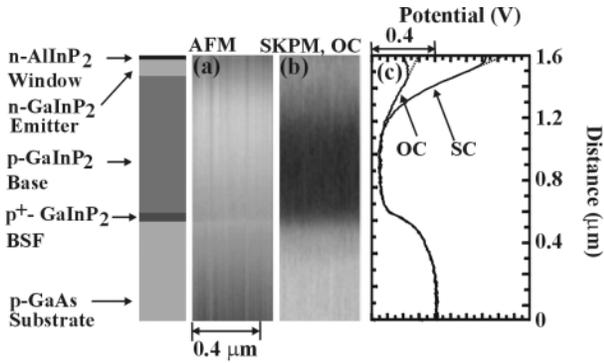
Figure 3. An AFM image (a) and the corresponding SKPM image (b) of GaInP$_2$ solar cells taken in OC. Potential profiles in OC and SC are given in (c).

We calculated the band diagram (Fig. 4) of the device bulk in thermal equilibrium state by solving Poisson's equation using the finite element method. The SKPM measures the electrochemical potential of the sample surface, and it is the work function in thermal equilibrium state. Because the E$_F$ is constant throughout the sample, the work function follows the profile of the vacuum level. The diagram is for electrons that have a negative charge, and the measured potential should be compared with the mirror image of the vacuum level, as indicated by "Potential" in Fig. 4. At the interface between the GaAs substrate and the p$^+$-GaInP$_2$ back surface field (BSF) layer, there is a potential decrease (~330 meV) because of the offsets of both conduction band and valence band between the two materials. At the interface between the p$^+$-GaInP$_2$ BSF and the p-GaInP$_2$ base layers, the potential increases slightly (~60 meV) due to the different doping levels. At the p-n junction, there is a big potential increase close to the value of the GaInP$_2$ band gap (~1.8 eV). Finally, at the interface between the n-GaInP$_2$ emitter and n-AlInP$_2$ window layers, there is a discontinuity in the conduction band because of the band offset. Accordingly, the potential increases slightly at the interface.
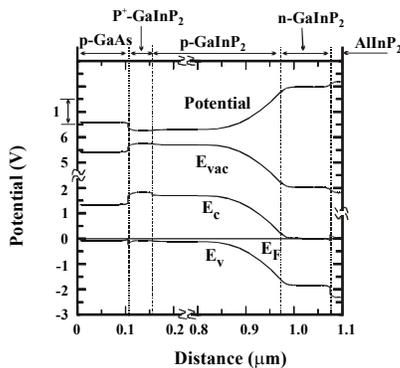

Figure 4. Calculated band diagram of the GaInP$_2$ device bulk in thermal equilibrium state. The dotted lines separate the different layers in the device structure.

We will compare the diagram with the measurement in SC. The measurement was performed with a leak of the laser light, and thus not in the thermal equilibrium state.

However, if the internal resistance of the device is small, the potential profile in SC should be similar to that of the thermal equilibrium state. The broad decrease in the potential [Fig. 3(c)] can be assigned to the potential drop at the GaAs/GaInP$_2$ interface. We did not observe the small potential dip on the BSF layer (Fig. 4). This may be due to inadequate spatial and/or energy resolutions of the SKPM performed at room temperature. If the measurement cannot probe the small dip, the measured potential decrease would correspond to the potential difference between the GaAs substrate and the GaInP$_2$ base layer, and the value in the band diagram is 330-60 = 270 meV. The difference (~80 meV) between the measurement (~350 meV) and the diagram (270 meV) is associated mainly with the different doping levels of the base layer and the substrate (~60 meV). This implies that the E$_F$ on the cleaved surface is pinned at similar positions above the valance band maximum for the GaInP$_2$ base layer and the GaAs substrate. From the measured potential (~350 meV), the E$_F$ pinning position of the p-type GaAs(110) surface (~0.88 eV below the conduction band minimum) [5], and the conduction band offset between GaInP$_2$ and GaAs (~60 meV), we suggest that the surface E$_F$ position of the p-type GaInP$_2$ material is at ~1.29 eV below the conduction band minimum. The increase in potential at the p-n junction is much smaller than that in the band diagram. This is also due possibly to the surface E$_F$ pinning. Surface E$_F$ may be pinned at different energy locations between n- and p-type materials due to electron- or hole-trap-like surface states. From the potential measurement (~0.78 eV) and the surface E$_F$ position of the p-type material, the surface E$_F$ for n-type GaInP$_2$ is pinned at ~0.51 eV below the conduction band minimum.

5. GaInP2/GaAs Tandem Cells

Figure 5 shows the device structure of the GaInP$_2$/GaAs tandem cell, an AFM image [Fig. 5(a)], and the corresponding SKPM image taken in SC [Fig. 5(b)]. For the potential profiles [Fig. 5(c)] taken in SC and OC, the potential shows broad decreases near the p-n junction of the bottom cell and the tunneling junction. The decrease in OC (~800 mV) is slightly deeper than in SC (~700 meV). Around the top p-n junction, the potential increases steeply in SC and slowly in OC, similar to the case of the GaInP$_2$ single-junction cell. Under SC, if we illuminate the sample from the front surface of the device using a short-pass filter that cuts off light with photon energies smaller than the band gap of the top cell, the shape of the potential profile changes dramatically even at a small light intensity of I_{top}=0.32 mW/cm^2 [see Fig. 5(c)]. The broad decrease around the bottom junction becomes a peak, and the steep increase at the top junction becomes flat. In the case of the single-junction cell, the shape of the potential profile did not change significantly in SC when a light was irradiated on the sample. However, in the tandem cell, which is essentially two serially connected diodes, the profile of the potential changes dramatically.

If the light from the halogen lamp is absorbed by the top cell, the minority carriers in the p-layer of the top cell (electrons) are excited and drift through the top p-n junction

3

and the front and back contacts of the device to the p-layer of the bottom cell, and the majority carriers of the top p-layer (holes) drift to the n-layer of the bottom cell through the tunneling junction. The electrons (holes) from the top cell combined with majority-carrier holes (electrons) in the p (n) layer of the bottom cell, and more dopant ions with negative (positive) charges on the p (n) layer of the bottom junction widen the depletion region of the p-n junction. If no photons, or fewer photons than are absorbed by the top cell, are absorbed in the bottom cell, the extra charges accumulated on the bottom junction cannot be carried through the bottom junction, and the accumulation of charge exerts a reverse-bias voltage on the bottom cell. This raises the potential in the bottom junction and induces the potential peak together with the potential decrease in the tunneling junction. The potential increase in the bottom junction is compensated by the flattening of the top-junction potential, which is induced by the drift of photo-excited carriers in the junction. Because the carrier flow is blocked in the bottom junction, the peak position of the profile may correspond to the boundary between the bottom and tunneling junctions, shown by the horizontal line in Fig. 5. In this way, we were able to determine the structure dimensions of the device.
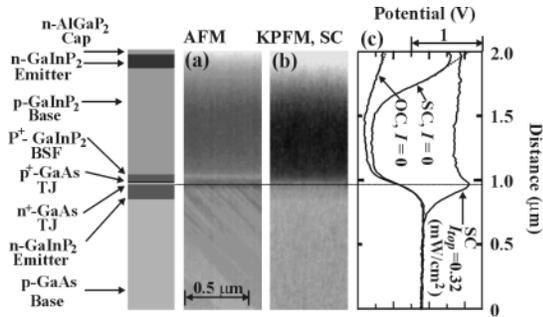

Figure 5. An AFM image (a), the corresponding SKPM image in SC (b), and potential profiles (c) taken on a GaInP$_2$/GaAs tandem cell. Potential profile taken in SC with an illumination of 0.32 mW/cm^2 is also shown in (c).

In the band diagram (Fig. 6) of the bulk at the thermal equilibrium state, the potential increase on the bottom junction is close to the p-layer's band gap (GaAs, ~1.42 eV). The potential decrease (1.56 eV) in the tunneling junction is slightly larger than the GaAs band gap because of the conduction band offset (0.14 eV) between GaAs and the disordered GaInP$_2$ BSF layer of the top cell. On the BSF layer, the potential shows a small dip (60 meV) that is like the case of GaInP$_2$ single-junction cell. The band diagram from the BSF to the top window layer is identical to the case of the single-junction cell. In the band diagram, the potential shows a saddle shape around the bottom and the tunneling junction that is ~0.2 μm in width and ~1.4 eV in height. However, we measured a decrease of potential in this region. The reason is possibly related to the flattening of the bottom p-n junction that is caused by the laser light. Leak of the laser light irradiates on the cross sections of the sample. Because the band gap of the bottom junction is smaller than that of the top junction, the absorption coefficient of the

bottom junction at the laser wavelength can be larger than for the top cell. This induces the flattening on the bottom cell and the charge accumulation on the top cell, in contrast to the intentional illumination with photon energies greater than the band gap of top cell. The flattening of the bottom cell makes the decrease of the potential (~700 mV) steeper than that of the device/substrate interface of the GaInP$_2$ single-junction cell (~350 meV, see Fig. 3). The charge accumulation on the top junction makes the increase (~1.30 V) steeper than that of the single-junction cell (~0.78 eV).
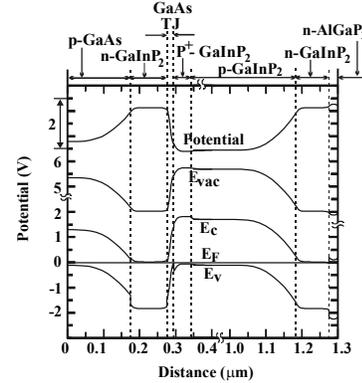

Figure 6. Calculated band diagram of a GaInP$_2$/GaAs tandem cell bulk in thermal equilibrium state.

6. Summary

We have applied SKPM to the characterization of photovoltaic devices, and have obtained useful information about the electrical properties of the devices. From the potential measurement for CIGS, the p-n junction is suggested to be a buried homojunction, located 30-80 nm from the CIGS/CdS interface in the CIGS film. For the GaInP$_2$ cell, the two potential features observed were assigned to the p-n junction and the potential barrier at the interface between the GaInP$_2$ base layer and the GaAs substrate. The potential on the p-n junction is photoactive, and that on the GaInP$_2$/GaAs interface is photo inactive. For the GaInP$_2$/GaAs tandem cell, when the sample was in SC, the potential distribution is unbalanced between the top and bottom junctions. If more (fewer) photons are absorbed by the top cell than the bottom cell, p-n junction flattening happened on the top (bottom) cell and the charge accumulations happened on the bottom (top) cell.

References

[1] C.-S. Jiang, H. R. Moutinho, J. F. Geisz, D. J. Friedman, and M. M. Al-Jassim, Appl. Phy. Lett. 81, 2569 (2002).
[2] C.-S. Jiang, F. S. Hasoon, H. R. Moutinho, H. A. Al-Thani, M. J. Romero, and M. M. Al-Jassim, Appl. Phys. Lett. 82, 127 (2003).
[3] C.-S. Jiang[a], H. R. Moutinho, D. J. Friedman, J. F. Geisz, and M. M. Al-Jassim, submitted to J. Appl. Phys.
[4] K. Ramanathan, R. Noufi, J. Granata, J. Webb, and J. Keane, Solar Energy Mat. Solar Cells 55, 15 (1998).
[5] K. J. Choi and J.-L. Lee, Appl. Phys. Lett. 74, 1108 (1999)

REPORT DOCUMENTATION PAGE

1. AGENCY USE ONLY (Leave blank)	2. REPORT DATE May 2003	3. REPORT TYPE AND DATES COVERED Conference Paper

4. TITLE AND SUBTITLE
Direct Measurement of Built-in Electrical Potential in Photovoltaic Devices by Scanning Kelvin Probe Microscopy

5. FUNDING NUMBERS
PVP3.3201

6. AUTHOR(S)
C.S. Jiang, H.R. Moutinho, F.S. Hasoon, H.A. Al-Thani, D.J. Friedman, J.F. Geisz, Q. Wang, M.J. Romero, and M.M. Al-Jassim

7. PERFORMING ORGANIZATION NAME(S) AND ADDRESS(ES)
National Renewable Energy Laboratory
1617 Cole Blvd.
Golden, CO 80401-3393

8. PERFORMING ORGANIZATION REPORT NUMBER
NREL/CP-520-33528

9. SPONSORING/MONITORING AGENCY NAME(S) AND ADDRESS(ES)

10. SPONSORING/MONITORING AGENCY REPORT NUMBER

11. SUPPLEMENTARY NOTES

12a. DISTRIBUTION/AVAILABILITY STATEMENT
National Technical Information Service
U.S. Department of Commerce
5285 Port Royal Road
Springfield, VA 22161

12b. DISTRIBUTION CODE

13. ABSTRACT *(Maximum 200 words)*
We report on direct measurements of the built-in electrical potential in Cu(In,Ga)Se2, GaInP2 single-junction, and GaInP2/GaAs tandem-junction solar cells, by using scanning Kelvin probe microscopy. Potential profiles on cross sections of the devices were measured quantitatively and spatially resolved in open and short circuit, under and without illuminations, with selective photon energies matching the band gaps of the junctions. The measurements provide valuable information about the electrical properties of the devices and are useful for understanding the performance and improving the design of solar cells.

14. SUBJECT TERMS
CIGS; direct measurement; built-in electrical potential; III-V solar cells; tandem junction

15. NUMBER OF PAGES

16. PRICE CODE

17. SECURITY CLASSIFICATION OF REPORT Unclassified	18. SECURITY CLASSIFICATION OF THIS PAGE Unclassified	19. SECURITY CLASSIFICATION OF ABSTRACT Unclassified	20. LIMITATION OF ABSTRACT UL

NSN 7540-01-280-5500